Bull. Plankton Eco-Eng. Res. 1: 32-46, 2021

プランクトン工学研究

Magnesium-modified biochars for nitrate adsorption and removal in continuous flow system

Joo Yun Qi and Shinjiro Sato*

Graduate School of Science and Engineering, Soka University, 1-236 Tangi-machi, Hachioji-shi, Tokyo, 192-8577, JAPAN
** Corresponding author: ssato@soka.ac.jp*

Received April 30 2021, Accepted May 14 2021

Abstract Excess utilization of chemical fertilizers in agriculture has caused nitrate pollution to groundwater and watershed, which has raised urgent need for effectively removing nitrate from water. Biochar has been suggested as one of the most promising adsorbent materials to remove nitrate from aqueous solution. However, adsorption capacity of pristine biochar is limited; therefore, several modification methods have been proposed to improve the adsorption capacity of biochar for nitrate. Therefore, the objectives of this study were to evaluate effects of magnesium (Mg)-modified biochars on the adsorption capacity for nitrate and removal efficiency as the sole filter media in a continuous flow system (biofilter). Pristine biochars were pyrolyzed at 550°C from oak sawdust (OS) and water hyacinth (WH), and Mg-modified biochars were produced by soaking feedstock in $MgCl_2$ solution followed by pyrolysis at the same temperature as the pristine biochars (OS/Mg and WH/Mg, respectively). Mg-modified biochars showed 84%–89% greater adsorption capacity for nitrate than pristine biochars. The highest adsorption capacity for nitrate was 19.1 mg g^{-1} obtained from WH/Mg biochar. Flow direction in the biofilter did not affect nitrate removal efficiency of biochar, but slower flow speed was more efficient because nitrate had more retention time to find adsorption sites on biochar surface. When used in a continuous flow system, the total amount of nitrate removed by WH/Mg biochar in the biofilter represented 27%–30% of the maximum adsorption capacity of the biochar depending on flow direction and speed. Optimization of biofilter structure (size and packing layer) and flow mechanics (flow direction and speed) for the maximum nitrate removal by biochar needs to be considered when used in the continuous flow system.

Keywords: biochar; biofilter; Langmuir; nitrate; water hyacinth

1. Introduction

At present, it is common to use chemical and animal manure fertilizers in agriculture to provide sufficient nutrients and organic matter to soils, so as to improve soil fertility and crop productivity. However, chemical fertilizers are one of the major sources of nitrate (NO_3^-) pollution in groundwater, and subsequently watersheds. Nitrate from the chemical fertilizers are highly soluble in water and cannot bind well with soil particles (Zhang et al. 2012). As a result, it can enter groundwater and surface water easily with rainfall. Further, high concentration of nitrate in drinking water can give rise to harmful

effects on human health, especially in infants, for example causing blue baby syndrome (Hafshejani et al. 2016).

Biofiltration or bioretention system is one of the most promising water recycling and reuseable systems. These systems have been widely utilized in developing countries (Guan et al. 2020). Moreover, the systems are chemical-free and passive methods for capturing and treating wastewater at source, which have proven to be effective in removing heavy metals, hydrocarbon, suspended solids, and phosphorus (Bratieres et al. 2008; Jay et al. 2019; Mahmoud et al. 2019). However, a number of studies have reported that the removal performance for nitrate was often limited due to low anion exchange capacity of soils (Hsieh & Davis, 2005; Davis, 2008; Line & Hunt, 2009). Therefore, for nitrate removal, carbon amendments such as crop residues, woodchips, sawdust, and biochars have been proposed (Shrestha et al. 2018; Jia et al. 2019). However, utilization of biochar as the sole biofilter to remove nitrate from water has not been fully investigated.

Biochar is a porous, carbon-rich solid product derived from thermal conversion of biomass under limited oxygen or anaerobic conditions (Inyang & Dickenson, 2015). Biochars derived from agricultural wastes and woody materials have shown effectiveness at removing nitrate (Zhang et al. 2012). Research trends about utilization of biochars have shifted from agriculture- and soil science-related fields such as organic fertilizer and soil amendment to environmental applications such as phytoremediation agent to fix heavy metals in soils and adsorbent to remove impurities from water. However, efficiency of biochars in the environmental application largely depends on adsorption capacity of biochar for adsorbate, and is often restricted due to its limited adsorption capacity of pristine biochar (Ahmed et al. 2016).

The limited adsorption capacity of pristine biochars can be overcome by synthesizing nano-composite biochars (called as functional or enhanced biochars) to improve physicochemical properties of biochars. Conventionally, the nano-composite biochars can be classified into three categories: functional nanoparticles-coated biochar, magnetic biochar, and metal-oxide composite biochars (Tan et al. 2016). The metal-oxide composite biochar can be produced by pretreating biomass with chemical reagent before pyrolysis. In general, metal salts are chosen as the chemical reagent for the pretreatment of biomass. The metal ions may attach onto the surface or enter into the interior of biomass during metal-salt solution biomass soaking. The metal ions then transform into nano metal-oxide, and subsequently the biomass impregnated with metal ions become nano-composite biochars after pyrolysis (Yao et al. 2013). Among them, magnesium (Mg)-composite biochars have shown excellent adsorption capacity to remove phosphate and nitrate from water (Yao et al. 2011). However, the maximum adsorption capacity and dynamics in a continuous flow system using nano metal-oxide composite biochars for nitrate removal have not been fully examined to date.

Water hyacinth (*Eichhornia crassipes*) is among the most noxious, dreadful, and invasive floating aquatic weeds in the world producing 140 million daughter plants annually and extending to 1.4 km^2 of cover water area with 28,000 t of fresh biomass (Ruan et al. 2016). The plant brings about serious environmental and socioeconomic problems, including ecological imbalance in lakes and clogging in navigation and irrigation systems (Gaurav et al. 2020). Attempts using chemical and mechanical

means have been made to remove water hyacinth from natural water bodies, which eventually are often to no avail. By contrast, in recent decades, there are a number of studies reported that the plant has demonstrated its potential for the phytoremediation of nitrogen, fecal bacteria, suspended solids, heavy metals, dyes, and organic matter in contaminated wastewaters and surface waters (Rezania et al. 2015). However, little research has focused on utilizing water hyacinth as a feedstock to produce biochar in removal of nitrate from water bodies.

Therefore, the objectives of this study were to evaluate (1) the maximum adsorption capacity of Mg-modified biochar for nitrate and (2) nitrate removal efficiency of Mg-modified biochar as the sole filter media in biofilter in continuous flow system.

2. Materials and methods

2.1. Preparation and analyses of biochars

Oak sawdust (*Quercus*) and water hyacinth were used as feedstock and dried in an oven at 95°C prior to pyrolysis. Pristine biochars (OS and WH, respectively) were obtained from pyrolysis in a covered ceramic crucible under oxygen-limiting condition in a muffle furnace with increasing rate of 5°C min^{-1} and retention time of 2 h at the maximum temperature of 550°C. To synthesize Mg-modified biochars (OS/Mg and WH/Mg, respectively), firstly 30.5 g of $MgCl_2 \cdot 6H_2O$ was dissolved in 300 mL of ultrapure water, into which 10 g of each feedstock was soaked for 4 h. The mixture of biomass and $MgCl_2$ were then oven-dried at 95°C to remove the water. The Mg-modified biochars were obtained from the same pyrolysis procedure as the pristine biochars. After cooling, the biochars were shaken with ultrapure water overnight at 160 strokes min^{-1} to wash away the impurities, filtered with Whatman No.1 filter paper, dried in the oven at 95°C, grounded and sieved to ≤ 500 μm and 500–2000 μm for adsorption and biofilter experiments, respectively.

Physicochemical properties of the biochars were analyzed for pH in a 1:10 biochar:deionised water (w/v) suspension (Singh et al. 2017); electrical conductivity in a 1:20 biochar:deionized water (w/v) suspension (Singh et al. 2017); cation exchange capacity (Graber et al. 2017); total C (TC), H, and N (TN) by Dumas dry oxidation method (Dumas 1930); and fixed C, volatile matter, and ash contents by thermal gravimetric analysis (Antal et al. 2000).

Specific surface area and pore size distribution of the biochars were measured by N gas adsorption at 77 K using Advanced Systems Analysis Program (ASAP 2010, Micrometritics). The Brunauer Emmett Teller (BET) method (Brunaueret al. 1938) was used to estimate the surface areas (S_{BET}). Total pore volumes (V_{total}) was estimated from the amount of N adsorbed at a relative pressure. Micropore volume (V_{mic}) was estimated by the t-plot method, and macropore and mesopore volumes ($V_{macro+meso}$) were estimated by difference of V_{total} and V_{mic}. After drying at 105°C for 24h, the biochar surface was observed by using Scanning Electron Microscopy (SEM) for all biochar samples before nitrate adsorption.

Fourier transform infrared (FTIR) spectra of the biochars were conducted by an FTIR instrument (IRPrestige-21 FTIR-8400S, Shimadzu) to analyze the surface functional groups for all biochar samples before nitrate adsorption, and only WH and WH/Mg biochar samples after nitrate adsorption (OS and OS/Mg biochar samples were not recovered after nitrate adsorption experiment).

2.2. Biochar adsorption kinetic and isotherm for nitrate

Nitrate solution for the adsorption experiments was prepared by using $NaNO_3$. For the adsorption kinetic experiment, the initial solution pH was adjusted to 2.0 with 1.0 M HCl or 0.05 M NaOH. 50 mg of biochar were added into a 50 mL centrifuge tube with 25 mL of 10 mg L^{-1} of nitrate solution. The tubes were shaken in a horizontal shaker at 160 strokes min^{-1} at room temperature with different shaking time intervals of 15, 30, 45, 60, 120, 240, and 1440 min. After each shaking time, the mixtures were filtered with Whatman No.1 filter paper followed by 0.45 μm pore size nylon membrane. The concentration of nitrate in the filtrate was measured using an auto-analyzer, and the adsorbed nitrate was calculated by difference from the initial concentration.

Adsorption kinetic results were described as the following pseudo-first order (Eq. 1) and pseudo-second order rate models (Eq. 2).

$$q_t = q_e(1 - e^{-k_1 t}) \quad (1)$$

$$q_t = \frac{q_e^2 k_2 t}{1 + q_e k_2 t} \quad (2)$$

where q_t (mg g^{-1}) and q_e (mg g^{-1}) were the amount of nitrate adsorbed by biochar at t shaking time and at equilibrium, respectively; t (min) was the shaking time; and k_1 (min^{-1}) and k_2 (g mg^{-1} min^{-1}) were the pseudo first and pseudo second order rate constants, respectively. The initial adsorption rate h (mg g^{-1} min^{-1}) was calculated by using the pseudo-second order kinetic parameters (Eq. 3).

$$h = q_e^2 k_2 \quad (3)$$

The initial concentration of nitrate was prepared as 0, 10, 20, 50, 80, 100, 200, and 300 mg L^{-1} for the adsorption isotherm experiment and adjusted pH to 2.0 with 1.0 M HCl or 0.05 M NaOH. 50 mg of biochar were added into a 50 mL centrifuge tube with 25 mL of each nitrate concentration solution. The tubes were shaken in the horizontal shaker at 160 strokes min^{-1} at room temperature for 1440 min. After shaking, the mixtures were filtered with Whatman No.1 filter paper followed by 0.45 μm pore size nylon membrane. The concentration of nitrate in the filtrate was measured using the auto-analyzer, and the adsorbed nitrate was calculated by difference from the initial concentration.

Adsorption isotherm results were fit with the following Langmuir (Eq. 4) and Freundlich adsorption isotherm models (Eq. 5).

$$q_e = \frac{K_L C_e q_m}{1 + K_L C_e} \quad (4)$$

$$q_e = K_F \times C_e^{\frac{1}{n}} \quad (5)$$

where q_e (mg g^{-1}) was the amount of nitrate adsorbed by biochar at equilibrium; C_e (mg L^{-1}) was the nitrate concentration in the solution at equilibrium; q_m (mg g^{-1}) was the maximum adsorption capacity; K_L (L mg^{-1}) and K_F were the Langmuir and Freundlich constant related to adsorption capacity, respectively; and n was the dimensionless adsorption constant related to the surface heterogeneity.

2.3. Biofilter removal of nitrate in continuous flow system

Polyvinyl chloride pipes (1.5 cm internal diameter and 12 cm length) were connected with rubber stoppers to build a model biofilter (Fig. 1). Glass wool was inserted at both ends (3 cm) of a biofilter with 1.382 g of biochar sample inside (5 cm) to prevent the biochar from washing out. The biofilters were then tapped by hand after each layer was poured to ensure no stratification

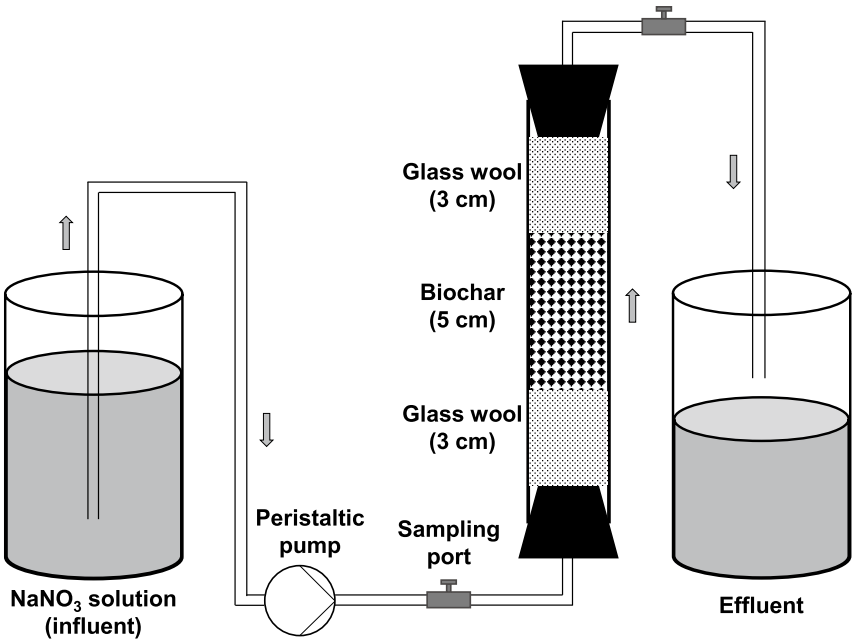

Figure 1. Schematic diagram of biofilter flow system for nitrate removal (upward flow configuration).

in the packed media. After packing, 300 mL ultrapure water was fed into all the biofilters (arranged in an upward flow configuration) using peristaltic pump with the speed of 50 mL h^{-1} for 6 h to saturate the biofilter with water and remove air space inside the biofilter.

WH/Mg was the only biochar being used in the biofilter experiment for nitrate removal. The experiment was carried out with four different treatments in two different flow directions (upward and downward) and two different flow speeds (50 and 100 mL h^{-1}) to assess the effect of biochar removal capacity. A 5.83 mg L^{-1} nitrate solution made from $NaNO_3$ was pumped through the biofilter for 60 h. Sampling time was 1, 2, 4, 8, 16, 24, 36, 48, and 60 h, and at each sampling time 20 mL was collected from influent before the biofilter (C_i) and effluent after the biofilter (C_e) from sampling ports. The pH of the solution was measured immediately after sampling, and nitrate concentration was then analyzed by using the auto-analyzer.

2.4. Statistical analyses

Statistical software STATISTICA 6.1 (StatSoft.Inc., Tulsa, OK, USA) was used to carry out the statistical analyses. Treatment effects were analyzed by one-way

Table 1. Physicochemical properties of biochars used in this study.

Biochar†	pH	Electric conductivity	Cation exchange capacity	Carbon	Hydrogen	Nitrogen	Fixed carbon	Volatile matter	Ash
		μS cm^{-1}	$cmol_c$ kg^{-1}	%	%	%	%	%	%
OS	7.88	320	17.3	77.3	1.81	0.180	76.5	21.6	1.88
OS/Mg	9.78	287	11.3	75.1	1.30	0.000	71.8	17.1	11.2
WH	9.58	1063	24.8	58.0	1.02	2.92	51.4	28.3	20.3
WH/Mg	9.66	552	25.3	59.6	1.24	2.61	58.5	22.6	18.9

† Biochars from oak sawdust (OS), water hyacinth (WH), Mg-modified OS (OS/Mg), and Mg-modified WH (WH/Mg) pyrolyzed at 550°C

Table 2 Surface areas and pore properties of biochars used in this study.

Biochar†	S_{BET}‡	S_{micro}‡	$S_{external}$‡	V_{total}⁋	V_{micro}⁋	$V_{macro+meso}$⁋
	$m^2\ g^{-1}$	$m^2\ g^{-1}$	$m^2\ g^{-1}$	$cm^3\ g^{-1}$	$cm^3\ g^{-1}$	$cm^3\ g^{-1}$
OS	323	249	73.9	0.163	0.115	0.0481
OS/Mg	270	195	75.9	0.196	0.089	0.107
WH	79.8	55.4	24.3	0.0564	0.025	0.0314
WH/Mg	276	177	98.0	0.204	0.204	0.122

† Biochars from oak sawdust (OS), water hyacinth (WH), Mg-modified OS (OS/Mg), and Mg-modified WH (WH/Mg) pyrolyzed at 550°C

‡ Specific surface area (S); total area (BET) = (micro area) + (external area)

⁋ Pore volume (V); total pore volume = (micro pore) + (macro+meso pores)

analysis of variance. A Tukey honestly significant difference analysis was performed for multiple comparisons of the treatment effects. Statistical significances were determined at $p < 0.05$.

3. Results

3.1. Biochar characterization

All biochars used in this study showed wide alkaline range (7.88–9.78; Table 1). Pristine WH biochar resulted in more alkaline pH than pristine OS biochar. Mg-modification caused more alkalinity after pyrolysis regardless of feedstock. OS feedstock (OS and OS/Mg) resulted in more TC and less TN, as well as more fixed C and less ash than WH feedstock (WH and WH/Mg). Mg-modification caused more ash content after pyrolysis regardless of feedstock.

OS and OS/Mg exhibited large total specific surface areas (323 and 270 $m^2\ g^{-1}$, respectively), of which 72%–77% were micro surface areas (249 and 195 $m^2\ g^{-1}$, respectively; Table 2). Pristine WH biochar showed much smaller S_{BET} and S_{micro} (79.8 and 55.4 $m^2\ g^{-1}$, respectively) than pristine OS biochar, but Mg-modification caused increase to both areas (276 and 177 $m^2\ g^{-1}$, respectively).

SEM surface images of the biochars showed morphological structures (Fig. 2). Both OS (Fig. 2a) and OS/Mg (Fig. 2b) possessed many clear porous structures, and it appeared that the pore size of OS/Mg was slightly larger than that of OS. On the other hand, the porous structures were limited in WH (Fig. 2c) and WH/Mg (Fig. 2d).

FTIR spectrum of WH and WH/Mg before and after nitrate adsorption revealed that a peak around 1734 cm^{-1} was possibly attributed to carbonyl functional groups C=O stretching vibration (Fig. 3), which may be responsible for nitrate adsorption site (Abdel-Ghani et al. 2016). A peak at around 1493 cm^{-1} in the spectra shows C=C groups in the biochars before and after nitrate adsorption (Kim et al. 2013). In addition, peaks around 881 cm^{-1} found in WH/Mg before and after adsorption should correspond to C–H stretching (Chen et al. 2015). A peak around 1636 cm^{-1} in OS and WH before nitrate adsorption (Fig. 3a) can be attributed to O–H stretching vibration of hydrogen-bonded groups and water molecules (Jung et al. 2015). Mg-O bonds (711 cm^{-1}) were present in the biochars before and after adsorption (Richardson & Braterman 2007).

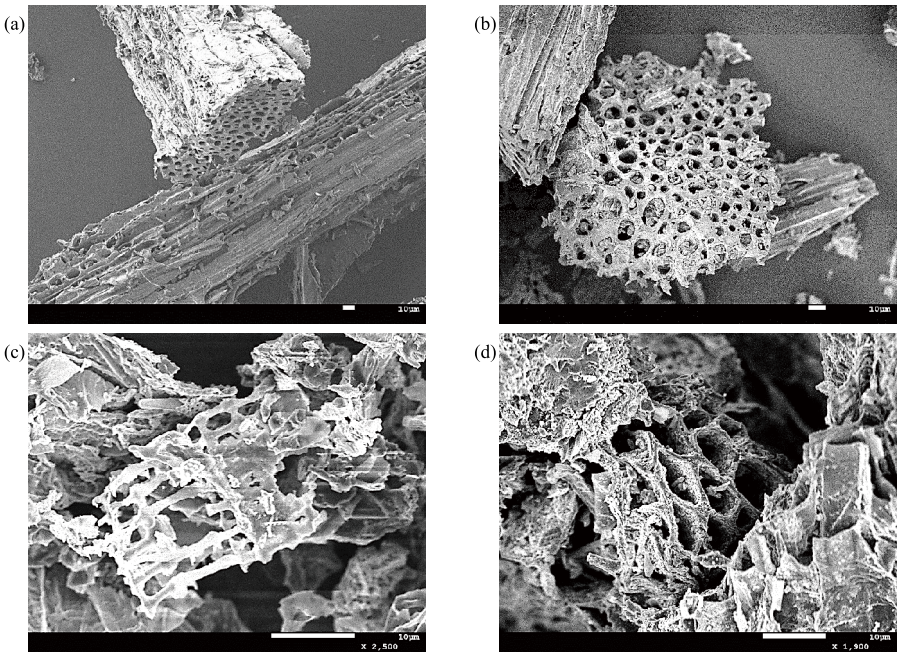

Figure 2. SEM surface image of (a) OS, (b) OS/Mg, (c) WH and (d) WH/Mg biochars.

3.2. Biochar adsorption kinetic and isotherm for nitrate

All biochars adsorbed nitrate quickly until 120 min of shaking, and reached quasi-equilibria with nitrate after 240 min, followed by full equilibria by 1440 min (Fig. 4). WH biochars showed higher adsorption capacity than OS biochars regardless of Mg-modification, and Mg-modified biochars showed more adsorption capacity than pristine biochars regardless of feedstock. The highest nitrate adsorption capacity was obtained from WH/Mg ($q_{e\ exp}$ = 9.04 mg g^{-1}; Table 3) at 1440 min shaking time.

Nitrate adsorption data of all biochars were better fit to the pseudo-second order kinetic model (R^2 = 0.956–0.999) compared to the pseudo-first order kinetic model (R^2 = 0.211–0.542; Table 3). The highest nitrate adsorption capacity calculated by the pseudo-second order model was obtained from WH/Mg ($q_{e\ 2}$ = 9.23 mg g^{-1}; Table 3). The initial adsorption rate h was 3.4–6.2 times higher for WH biochars than OS biochars, and the highest h was obtained from WH/Mg (0.278 mg $g^{-1}min^{-1}$; Table 3).

All biochars exhibited clear adsorption isotherms for nitrate (Fig. 5). The adsorption equilibrium was

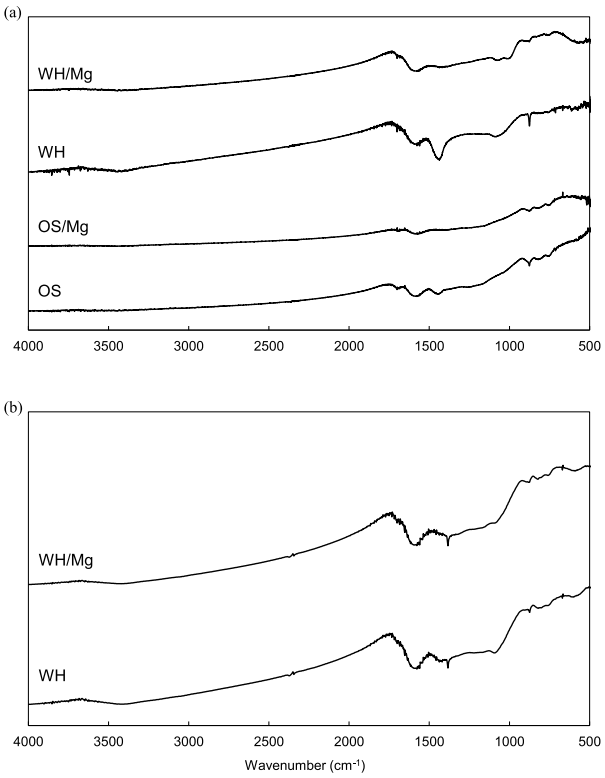

Figure 3. FTIR spectra of (a) OS, OS/Mg, WH, and WH/Mg biochars before nitrate adsorption and (b) WH and WH/Mg biochars after nitrate adsorption.

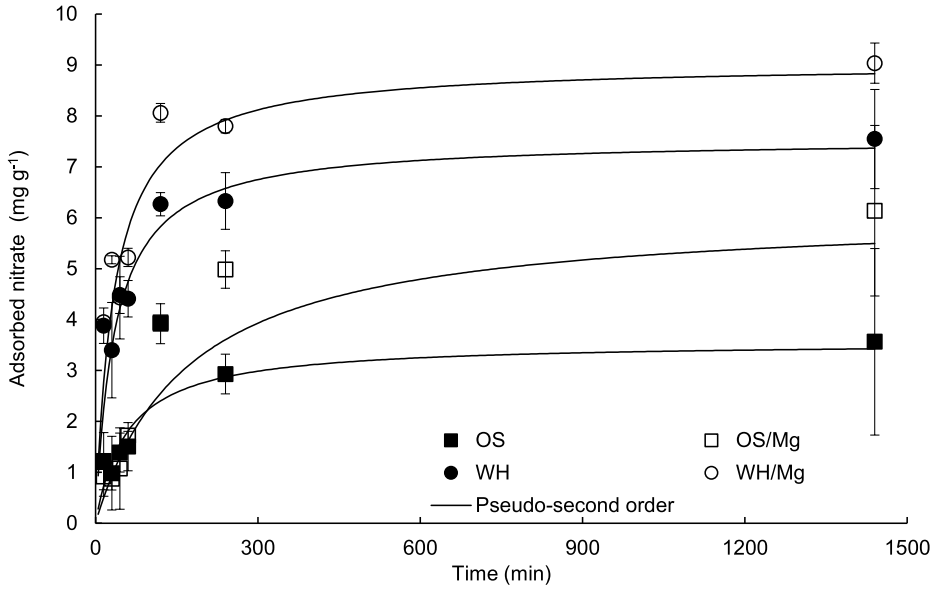

Figure 4. Adsorption kinetic of OS, OS/Mg, WH, and WH/Mg biochars for nitrate. Solid lines represent approximation by pseudo-second order kinetic model.

achieved at a concentration of around 200 mg L^{-1} for all biochars. The highest adsorption capacity was obtained from WH/Mg, whereas OS showed the lowest.

Both Langmuir and Freundlich adsorption isotherm models fit well with nitrate adsorption data of all biochars (R^2 = 0.893–0.983 and 0.954–0.991, respectively; Table 4). Comparing two models, the Freundlich model fit better with nitrate adsorption by OS/Mg, WH, and WH/Mg, while the Langmuir fit better with that by OS. The highest maximum adsorption capacity calculated by the Langmuir model (q_m) was 19.1 mg g^{-1} for WH/Mg, followed by 10.4 mg g^{-1} for WH, 9.68 mg g^{-1} for OS/Mg, and the lowest value of 5.11 mg g^{-1} for OS.

3.3. Biofilter removal of nitrate in continuous flow system

For both upward and downward flow directions, relative nitrate concentration in C_e to C_i (C_e/C_i) was almost 0 for the first 4 h regardless of flow speed (50 or 100 mL h^{-1}; Fig. 6). However, C_e/C_i values quickly increased to 0.358–0.437 for 8 h with 100 mL h^{-1}, while remaining at 0 with 50 mL h^{-1}, regardless of the flow direction. Then,

Table 3. Pseudo-first order and pseudo-second order kinetic model parameters for nitrate adsorption kinetic.

Biochar†	Pseudo-first order				Pseudo-second order			
	$q_{e\,exp}$‡	k_1	$q_{e\,1}$	R^2	k_2	$q_{e\,2}$	h	R^2
	mg g^{-1}	×10^{-3} min^{-1}	mg g^{-1}		×10^{-3} g mg^{-1} min^{-1}	mg g^{-1}	mg g^{-1} min^{-1}	
OS	3.56	0.486	1.72	0.211	4.83	3.71	0.0665	0.956
OS/Mg	6.14	1.05	3.82	0.542	0.967	6.83	0.0451	0.982
WH	7.55	0.781	2.70	0.453	3.74	7.72	0.223	0.999
WH/Mg	9.04	0.882	3.03	0.363	3.26	9.23	0.278	0.999

† Biochars from oak sawdust (OS), water hyacinth (WH), Mg-modified OS (OS/Mg), and Mg-modified WH (WH/Mg) pyrolyzed at 550°C

‡ The maximum adsorption capacity from the experiment at shaking time of 1440 min

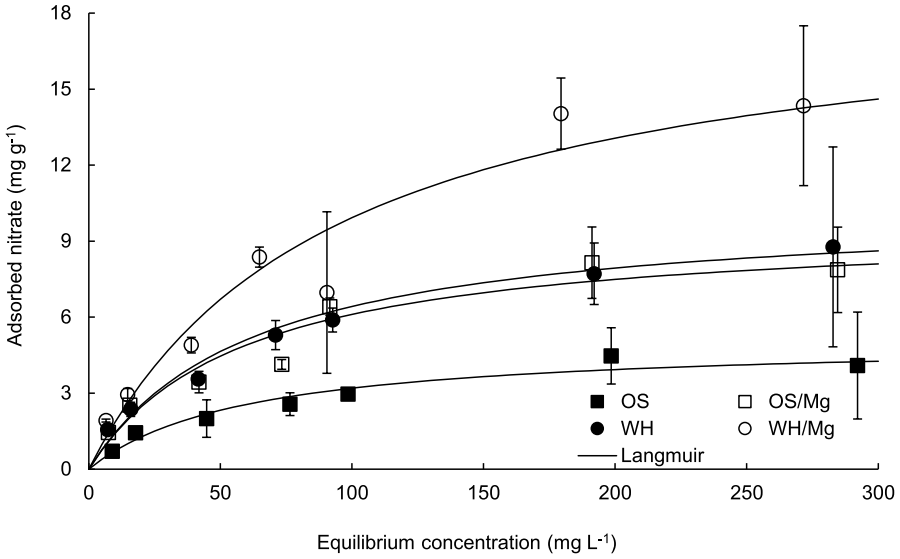

Figure 5. Adsorption isotherms of OS, OS/Mg, WH, and WH/Mg biochars for nitrate. Solid lines represent approximation by Langmuir adsorption isotherm model.

C_e/C_i values reached 0.978–1.00 for 36 h with 100 mL h^{-1}, while continuing to increase or remaining relatively constant with 50 mL h^{-1} even after 36 h, regardless of flow direction.

The final pH of the effluent with upward flow direction showed similar trends with time passing for both flow speeds (Fig. 6a). The final pH was around 9.0 in the beginning, quickly dropped to 2.3–2.5 for 8 h, and remained relatively constant for the rest of time. However, for the downward flow direction biofilter, the final pH quickly dropped from 9.0 to 2.4 for 4 h and remained relatively constant for the rest of time (Fig. 6b). The flow speed appeared to have no effects on pH change over time for both flow directions.

Table 4. Langmuir and Freundlich adsorption isotherm model parameters for nitrate adsorption isotherm.

Biochar†	Langmuir model			Freundlich model		
	K_L	q_m	R^2	K_F	n	R^2
	L mg^{-1}	mg g^{-1}		$mg^{1-(1/n)}$ $L^{1/n}$ g^{-1}		
OS	0.0167	5.11	0.972	0.285	2.00	0.954
OS/Mg	0.0170	9.68	0.953	0.607	2.10	0.956
WH	0.0161	10.4	0.983	0.621	2.08	0.991
WH/Mg	0.0107	19.1	0.893	0.659	1.77	0.972

† Biochars from oak sawdust (OS), water hyacinth (WH), Mg-modified OS (OS/Mg), and Mg-modified WH (WH/Mg) pyrolyzed at 550°C

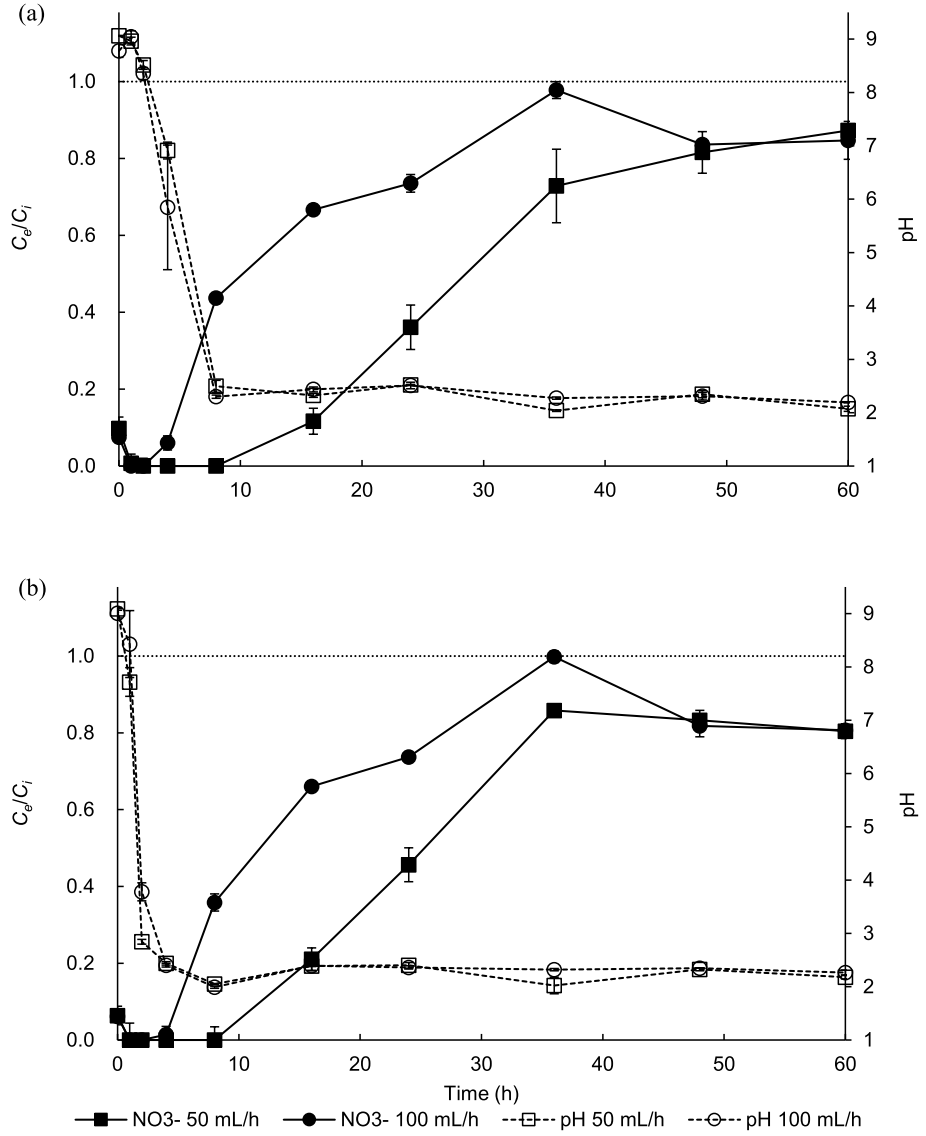

Figure 6. Relative nitrate concentration in effluent after the biofilter (C_e) to influent before the biofilter (C_i) (breakthrough curve) and effluent solution pH with (a) upward and (b) downward flow directions. A dotted line represents adsorption saturation point when C_e/C_i = 1.

4. Discussion

4.1. Nitrate adsorption kinetics

Adsorption kinetics can provide essential parameters about the reaction pathway and mechanism of the adsorption process (Xu et al. 2013). Better fit of biochars' nitrate adsorption results with the pseudo second-order than the pseudo first-order model (Table 3) can indicate that adsorption was governed by physicochemical composite reactions involving external liquid film diffusion, surface adsorption, and intraparticle diffusion (Tümsek & Avci, 2013). The maximum adsorption capacity of the biochars calculated by the pseudo second-order model ($q_{e\,2}$ = 3.71–9.23 mg g^{-1}) were almost same as those from the experiment at 1440 min shaking time ($q_{e\,exp}$ = 3.56–9.04 mg g^{-1}), and highest $q_{e\,2}$ was obtained from WH/Mg. The initial adsorption rate h values calculated by the pseudo-second order model showed better initial

performance by WH biochars compared to OS biochars, and the highest initial adsorption was obtained from WH/Mg. These results confirmed that Mg-modification particularly for WH biochar was effective to improve adsorption capacity of pristine biochar for nitrate. However, the optimum kinetic model for nitrate by biochars may be different depending on biochar properties such as biochar feedstock, production temperatures, and modification procedures if any. For example, the optimum kinetic model was pseudo-first order, pseudo-second order, and Elovich models for date-palm Mg/Al-modified biochar (Alagha et al. 2020), palm leaf residues non-modified biochar (Zare & Ghasemi-Fasaei 2019), and corncob $FeCl_3$-modified biochar (Long et al. 2019), respectively. Therefore, more detailed investigations are needed for better understanding on effects of different physicochemical properties of feedstock and/or production procedures of biochars on physicochemical mechanism for nitrate adsorption by biochars.

4.2. Nitrate adsorption isotherms

The adsorption isotherms of different biochars for nitrate showed better fitting results with the Freundlich than the Langmuir adsorption isotherm model except for OS biochar (Table 4), indicating reversible adsorption process where the biochar surface containing adsorption sites was heterogeneous and each site could hold several molecules in multilayers (Keränen et al. 2015; Zhen et al. 2015). Comparing the maximum adsorption capacity calculated by the Langmuir model, Mg-modification of biochars resulted in 1.89 and 1.84 times higher capacity than pristine biochars for OS and WH, respectively (Table 4). For nitrate adsorption, the mechanism may be controlled by multiple interactions such as fixation by ionic bonding with exchangeable cations from $MgCl_2$ and electrostatic attraction (Hale et al. 2013), which could have happened with Mg-modified biochars. On the other hand, an assumption of the Langmuir adsorption isotherm model is that the surface containing the adsorption sites is homogeneous and that each site can hold at most one molecule in thickness, also known as monolayer adsorption (Keränen et al. 2015). Therefore, the monolayer adsorption of nitrate on homogenous surface could have occurred for OS biochar without Mg-modification, thus reducing the maximum adsorption capacity.

The maximum adsorption capacity of OS biochar in this study (5.11 mg g^{-1}; Table 4) was comparable with that of OS biochar in other studies (8.94 mg g^{-1}; Wang et al. 2015). As seen in this study, improvement of the maximum adsorption capacity by Mg-modification was also seen in other studies. For example, a peanut shell biochar modified by Mg increased nitrate adsorption capacity to 94 mg g^{-1} (Zhang et al. 2012). However, when OS was modified by $LaCl_3$, the maximum adsorption capacity increased up to 100 mg g^{-1} (Wang et al. 2015). Therefore, the adsorption capacity of biochar for nitrate largely depends on types of feedstock, pyrolysis conditions, and most importantly modification procedures. The highest maximum adsorption capacity of biochar for nitrate found in the most recent literature may be 157 mg g^{-1} when apple branch biochar was modified by CO_2-activation plus Mg/Al-layered double hydroxides-modification (Wang et al. 2021).

4.3. Nitrate removal by biofilter

Relative nitrate concentration in C_e to C_i (C_e/C_i) represents how much nitrate was removed from solution (or adsorbed by biochar) in the biofilter, and shows 1 (one) when the biochar was saturated with nitrate (or reached the maximum adsorption capacity). The breakthrough curve of the biochar for nitrate showed that flow direction (upward or downward) did not seem

Table 5. Total nitrate removed by biofilter and relateive percentages to the maximum adsorption capacity of biochar.

Flow direction	Flow speed	Total nitrate flowed†	Total nitrate removed‡	Removed by biofilter⁋	Biochar saturated by nitrate⁗
	mL h^{-1}	mg	mg	%	%
Upward	50	17. 5	7.92	45%	30%
	100	35.0	8.74	25%	33%
Downward	50	17.5	7.20	41%	27%
	100	35.0	9.26	26%	35%

† Total amounts of nitrate pumped through the biofilter calculated as (flow speed, 50 mL h^{-1} × flow time, 60 h × influent nitrate concentration, 5.83 mg $L^{-1}\times10^{-3}$)

‡ Total amounts of nitrate removed by biofilter calcualted as difference of total nitrate flowed and total nitrate in effluent sampled after the biofilter

⁋ Percentages of total nitrate removed to total nitrate flowed calcualted as (total nitrate removed / total nitrate flowed × 100%)

⁗ Percentages of total nitrate removed to the maximum adsorption capacity of biochar for nitrate calculated as (total nitrate removed / the maximum adsorption capacity of biochar × 100%) where the maximum adsorption capacity of biochar was calculated as (the maximum adsorption capacity of WH/Mg biochar, 19.1 mg g^{-1}; Table 4 × biochar weight in the biofilter, 1.382 g)

to have significant effects on nitrate removal efficiency of biochar in the biofilter (Fig. 6). However, flow speed (50 or 100 mL h^{-1}) appeared to have affected removal efficiency of biochar for nitrate. Regardless of flow direction, C_e/C_i reached to 1 (biochar saturated with nitrate) at 36 h with 100 mL h^{-1}, while it had not reached 1 even at 60 h with 50 mL h^{-1}. The removal efficiency of biochars in the biofilter with slower flow speed was more efficient because nitrate had more retention time to find adsorption sites on the biochar surface allowing more nitrate being removed by the biochar. The breakthrough curve was also strongly dependent on the influent nitrate concentration; the higher the nitrate concentration, the faster the nitrate broke through and the resin was saturated (Keränen et al. 2015).

Total amounts of nitrate removed by the biofilter and their relative percentages to the maximum adsorption capacity of WH/Mg biochar were assessed for different flow direction and flow speed (Table 5). Total amounts of nitrate removed was calculated as the difference of total amounts of nitrate pumped through the biofilter (total nitrate flowed) and total amounts of nitrate in effluent sampled after the biofilter for 60 h. Total nitrate removed with upward flow direction resulted in 7.92 and 8.74 g, and with downward flow direction 7.20 and 9.26 g with 50 and 100 mL h^{-1} flow speed, respectively (Table 5). Percentages of total nitrate removed to total nitrate flowed (% removed by biofilter) were comparable between flow directions but different by flow speed: 41%–45% and 25%–26% for slow and fast flow speeds, respectively (Table 5). This result confimed again insignificant effects of flow direction on the nitrate removal of biochar in the biofilter, but noteworthy effects by flow speed. It appears clear from this study that faster flow speed could result in less retention time of nitrate with biochar, thus less adsorption or removal by the biofilter. Low nitrate removal percentages by the biofilter found in this study could be improved by slowing flow speed even more and/or widening the biofilter diameter to increase nitrate retention time with biochar in the biofilter. However, percentages of total nitrate removed to the maximum adsorption capacity

of biochar in the biofilter (% biochar saturated by nitrate) calculated as [the maximum adsorption capacity of WH/Mg biochar, 19.1 mg g^{-1}; Table 4 × biochar weight in the biofilter, 1.382 g] showed comparable with 27%–35% regardless of flow direction and flow speed (Table 5). This result implies that when used in the continuous flow system biochar could adsorb nitrate only around 30% of its maximum adsorption capacity regardless of flow direction and flow speed. The reduced adsorption capacity in the continuous flow system could be a result of reduced retention time of biochar with nitrate in the biofilter compared to 24 h of shaking time in tube for adsorption isotherm experiment and/or difference in adsorbed (saturated) fractions of biochar particles depending on location within the biofilter. Biochar particles closer to influent side of the biofilter may adsorb (be saturated with) more nitrate than those closer to effluent side of the biofilter. Therefore, switching flow directions during flowing period could overcome this shortcoming by utilizing biochar particles unsaturated with nitrate.

5. Conclusion

This study demonstrates the adsorption capacity of biochars produced from both oak sawdust and water hyacinth for removing nitrate from aqueous solution. Furthermore, Mg-modification of biochar was proven to be effective to improve adsorption capacity of biochar. The adsorption isotherms of biochars for nitrate were well fit with both Langmuir and Freundlich adsorption isotherm models. Water hyacinth Mg-modified biochar was also successfully used to remove nitrate from the continuous flow system (biofilter), but with limited removal efficiency. Optimization of biofilter structure (size and packing layer) and flow mechanics (flow direction and speed) for the maximum nitrate removal by biochar needs to be considered when used in the continuous flow system.

6. Acknowledgements

Authors are thankful to city governments of Gyoda and Kazo City for allowing to sample water hyacinth from parks. Authors acknowledge members of Laboratories of Restoration Ecology and Environmental Chemical Engineering at Soka University for analytical instruments. This research was supported by Private University Research Branding Project (PLANE3T) funded by MEXT, and Science and Technology Research Partnership for Sustainable Development (SATREPS) funded by Japan Science and Technology Agency (JST)/Japan International Cooperation Agency (JICA)(Grant Number JPMJSA2005).

References

Abdel-Ghani NT, El-Chaghaby GA, ElGammal MH, Rawash ESA (2016) Optimizing the preparation conditions of activated carbons from olive cake using KOH activation. New Carbon Mater 31: 492–500.

Ahmed MB, Zhou JL, Ngo HH, Guo W, Chen M (2016) Progress in the preparation and application of modified biochar for improved contaminant removal from water and wastewater. Bioresour Technol 214: 836–851.

Alagha O, Manzar MS, Zubair M, Anil I, Mu'azu ND, Qureshi A (2020) Comparative adsorptive removal of phosphate and nitrate from wastewater using biochar-MgAl LDH nanocomposites: Coexisting anions effect and mechanistic studies. Nanomaterials 10: 336.

Antal MJ, Allen SG, Dai X, Shimizu B, Tam MS, Gronli M (2000) Attainment of the theoretical yield of carbon from biomass. Ind Eng Chem Res 39: 4024–4031.

Bratieres K, Fletcher TD, Deletic A, Zinger Y (2008) Nutrient and sediment removal by stormwater biofilters: A large-scale design optimisation study. Water Res 42: 3930–3940.

Brunauer S, Emmtt PHH, Teller E (1938) Adsorption of gases in multimolecular layers. J Am Chem Soc 60: 309–319.

Chen J, Fan X, Jiang B, Mu L, Yao P, Yin H, Song X (2015) Pyrolysis of oil-plant wastes in a TGA and a fixed-bed reactor: Thermochemical behaviors, kinetics, and products characterization. Bioresour Technol 192: 592–602.

Davis AP (2008) Field performance of bioretention: Hydrology impacts. J Hydrol Eng 13: 90–95.

Dumas JBA (1831) Procedes de l'analyse organique. Ann Chim Phys 2: 198.

Gaurav GK, Mehmood T, Cheng L, Klemeš, JJ, Shrivastava DK (2020) Water hyacinth as a biomass: A review. J Cleaner Prod 277: 122214.

Graber ER, Singh B, Hanley K, Lehmann J (2017) "Determination of cations exchange capacity in biochar" In: Biochar. A guide to analytical methods (eds Singh B, Camps-Arbestain M, Lehmann J). CRC Press, Boca Raton, pp. 74–84

Guan P, Prasher SO, Afzal MT, George S, Ronholm J, Dhiman J, Patel RM (2020) Removal of *Escherichia coli* from lake water in a biochar-amended biosand filtering system. Ecol Eng 150: 105819.

Hafshejani LD, Hooshmand A, Naseri AA, Mohammadi AS, Abbasi F, Bhatnagar A (2016) Removal of nitrate from aqueous solution by modified sugarcane bagasse biochar. Ecol Eng 95: 101–111.

Hale SE, Alling V, Martinsen V, Mulder J, Breedveld GD, Cornelissen G (2013) The sorption and desorption of phosphate-P, ammonium-N and nitrate-N in cacao shell and corn cob biochars. Chemosphere 91: 1612–1619.

Hsieh CH, Davis AP (2005) Evaluation and optimization of bioretention media for treatment of urban storm water runoff. J Environ Eng 131: 1521–1531.

Inyang M, Dickenson E (2015) The potential role of biochar in the removal of organic and microbial contaminants from portable and reuse water: A review. Chemosphere 134: 232–240.

Jay JG, Tyler-Plog M, Brown SL, Grothkopp F (2019) Nutrient, metal, and organics removal from stormwater using a range of bioretention soil mixtures. J Environ Qual 48: 493–501.

Jia L, Gou E, Liu H, Lu S, Wu S, Wu H (2019) Exploring utilization of recycled agricultural biomass in constructed wetlands: Characterization of the driving force for high-rate nitrogen removal. Environ Sci Technol 53: 1258–1268.

Jung KW, Jeong TU, Hwang MJ, Kim K, Ahn KH (2015) Phosphate adsorption ability of biochar/Mg–Al assembled nanocomposites prepared by aluminum-electrode based electro-assisted modification method with $MgCl_2$ as electrolyte. Bioresour Technol 198: 603–610.

Keränen A, Leiviskä T, Hormi O, Tanskanen J (2015) Removal of nitrate by modified pine sawdust: Effects of temperature and co-existing anions. J Environ Manage, 147: 46–54.

Kim P, Johnson AM, Essington ME, Radosevich M, Kwon WT, Lee SH, Rials T, Labbé N (2013) Effect of pH on surface characteristics of switchgrass-derived biochars produced by fast pyrolysis. Chemosphere 90: 2623–2630.

Line DE, Hunt WF (2009) Performance of a bioretention area and a level spreader-grass filter strip at two highway sites in North Carolina. J Irrig Drain Eng 135: 217–224.

Long L, Xue Y, Hu X, Zhu Y (2019) Study on the influence of surface potential on the nitrate adsorption capacity of metal modified biochar. Environ Sci Pollut Res 26: 3065–3074.

Mahmoud A, Alam T, Rahman MYA, Sanchez A, Guerrero J, Jones KD (2019) Evaluation of field-scale stormwater bioretention structure flow and pollutant load reductions in a semi-arid coastal climate. Ecol Eng X 1: 100007.

Rezania S, Ponraj M, Talaiekhozani A, Mohmad SE, Din MFM, Taib SM, Sabbagh F, Sairan FM (2015) Perspectives of phytoremediation using water hyacinth for removal of heavy metals, organic and inorganic pollutants in wastewater. J Environ Manage

163: 125–133.

Richardson MC, Braterman PS (2007) Infrared spectra of oriented and nonoriented layered double hydroxides in the range from 4000 to 250 cm^{-1}, with evidence for regular short-range order in a synthetic Magnesium–Aluminum LDH with Mg:Al = 2:1 but not with Mg:Al = 3:1. J Phys Chem C 111: 4209–4215.

Ruan T, Zeng R, Yin XY, Zhang SX, Yang ZH (2016) Water hyacinth (*Eichhornia crassipes*) biomass as a biofuel feedstock by enzymatic hydrolysis. BioRes 11: 2372–2380.

Shrestha P, Hurley SE, Wemple BC (2018) Effects of different soil media, vegetation, and hydrologic treatments on nutrient and sediment removal in roadside bioretention systems. Ecol Eng 112: 116–131.

Singh B, Dolk MM, Shen Q, Camps-Arbestain M (2017) "Biochar pH, electrical conductivity and liming potential" In: Biochar. A guide to analytical methods (eds Singh B, Camps-Arbestain M, Lehmann J). CRC Press, Boca Raton, pp. 23–38

Tan X, Liu Y, Gu Y, Xu Y, Zeng G, Hu X, Liu S, Wang X, Liu S, Li J (2016) Biochar-based nano-composites for the decontamination of wastewater: A review. Bioresour Technol 212: 318–333.

Tümsek F, Avci Ö (2013) Investigation of kinetics and isotherm models for the acid orange 95 adsorption from aqueous solution onto natural minerals. J Chem Eng Data 58: 551–559.

Wang T, Zhang D, Fang K, Zhu W, Peng Q, Xie Z. (2021) Enhanced nitrate removal by physical activation and Mg/Al layered double hydroxide modified biochar derived from wood waste: Adsorption characteristics and mechanisms. J Environ Chem Eng 9: 105184.

Wang Z, Guo H, Shen F, Yang G, Zhang Y, Zeng Y, Wang L, Xiao H, Deng S (2015) Biochar produced from oak sawdust by Lanthanum (La)-involved pyrolysis for adsorption of ammonium (NH_4^+), nitrate (NO_3^-), and phosphate (PO_4^{3-}). Chemosphere 119: 646–653.

Xu X, Gao B, Tan T, Zhang X, Yue Q, Wang Y, Li Q (2013) Nitrate adsorption by stratified wheat straw resin in lab-scale columns. Chem Eng J 226: 1–6.

Yao Y, Gao B, Chen J, Yang L (2013) Engineered biochar reclaiming phosphate from aqueous solutions: Mechanisms and potential application as a slow-release fertilizer. Environ Sci Technol 47: 8700–8708.

Yao Y, Gao B, Inyang M, Zimmerman AR, Cao X, Pullammanappallil P, Yang L (2011) Biochar derived from anaerobically digested sugar beet tailings: Characterization and phosphate removal potential. Bioresour Technol 102: 6273–6278.

Zare L, Ghasemi-Fasaei R (2019) Investigation of equilibrium isotherm and kinetic modeling to asses sorption characteristics of nitrate onto palm leaf biochar. Iran J Chem Chem Eng 38: 143–153.

Zhang M, Gao B, Yao Y, Xue Y, Inyang M (2012) Synthesis of porous MgO-biochar nanocomposites for removal of phosphate and nitrate from aqueous solution. Chem Eng J 210: 26–32.

Zhen Y, Ning Z, Shaopeng Z, Yayi D, Xuntong Z, Jiachun S, Weiben Y, Yuping W, Jianqiang C (2015) A pH- and temperature-responsive magnetic composite adsorbent for targeted removal of nonylphenol. ACS Appl Mater Interfaces 7: 24446–24457.